DOI https: //doi. org/10.1007/s11595-023-2662-3

In Situ Reaction Strengthening and Toughening of $B_4C/TiSi_2$ Ceramics

XIA Tao[2], TU Xiaoshi[2*], ZHANG Fan[1,2*], ZHANG Jinyong[2], REN Lin[3]

(1. Hubei Longzhong Laboratory, Wuhan University of Technology, Xiangyang Demonstration Zone, Xiangyang 441000, China; 2. State Key Laboratory of Advanced Technology for Materials Synthesis and Processing, Wuhan University of Technology, Wuhan 430070, China; 3. School of Science, Wuhan University of Technology, Wuhan 430070, China)

Abstract: B_4C-SiC-TiB_2 ceramics were prepared by *in situ* reactive hot-pressing sintering with $TiSi_2$ as an additive. The reaction pathways of $TiSi_2$ and B_4C were investigated. The sintering was found to be a multi-step process. The reaction started at approximately 1 000 ℃, and TiB_2 was formed first. Part of Si and C started to react at 1 300 ℃, and the unreacted Si melted at 1 400 ℃ to form a liquid phase. $TiSi_2$ predominantly affected the intermediate sintering process of B_4C and increased the sintering rate. Due to the unique reaction process of $TiSi_2$ and B_4C, a large number of aggregates composed of SiC and TiB_2 were generated. The results showed that composite ceramics with the optimal flexural strength of 807 MPa, fracture toughness of 3.2 MPa·$m^{1/2}$, and hardness of 32 GPa, were obtained when the $TiSi_2$ content was 10 wt%.

Key words: *in situ* reaction; hot pressing sintering; $TiSi_2$; B_4C composite ceramics; reaction mechanism

1 Introduction

Boron carbide has a low density (2.52 g/cm^3) and high hardness, good chemical stability, high neutron absorption, and other excellent characteristics, making it a vital engineering structural material. Owing to the stronger covalent bonds in B_4C, the dislocation movements do not occur easily when subjected to external forces. Therefore, B_4C exhibits inferior fracture toughness and flexural strength of 2.2 MPa·$m^{1/2}$ and 400 MPa, respectively[1,2]. Various processes have been attempted to improve the high brittleness, low strength, and difficult sintering of B_4C. After comprehensive research, it has been proven that the second-phase toughening method is an effective process to prepare high-performance B_4C ceramics. The materials typically used as the second phase are CrB_2, ZrB_2, W_2B_5, BN, MoB_2 and so on[3-8].

The properties of the second phase have a significant influence on the composite material, which makes the selection of the second phase crucial. The hardness and density of SiC and TiB_2 are similar to those of B_4C[9,10]. The introduction of SiC can improve the toughness and high-temperature oxidation resistance of B_4C ceramics[11]. TiB_2 can improve the final density, hardness, and wear resistance of B_4C[12]. Because of the thermal expansion mismatch between the TiB_2 particles and the B_4C matrix, it is easy to generate residual stress at the grain boundary during the cooling process, causing microcracks to deflect and achieve the effect of toughening[13]. The introduction of TiB_2 can also improve the machinability of B_4C owing to its high electrical conductivity[14]. The *in-situ* reaction sintering method can increase the sintering activity of B_4C and lower the sintering temperature. The second phase produced during sintering is often smaller than the directly added second phase, which also helps to improve the mechanical properties of B_4C composites[15].

In this study, $TiSi_2$ was used as an additive to react with B_4C *in situ* during sintering to obtain SiC and TiB_2. The advantage of this method is that two second phases can be introduced simultaneously, and no gas is generated. We analyzed in detail the reaction pathways of $TiSi_2$ and B_4C in the sintering process and studied the effect of $TiSi_2$ addition on the sintering process of B_4C, which provided a new idea for the low-cost preparation of high-performance B_4C ceramics.

(Received: Jan. 26, 2022; Accepted: Oct. 21, 2022)

XIA Tao(夏涛): E-mail: xt1222@whut.edu.cn

*Corresponding author: TU Xiaoshi(涂晓诗): E-mail: tuxiaoshi@whut.edu.cn; ZHANG Fan(张帆): Assoc. Prof.; E-mail: zhfan@whut.edu.cn

Funded by the National Natural Science Foundation of China(No.52002299)

2 Experimental

B_4C (D_{50}=1.0 μm, purity 99.9%, H. C. Stark Inc, Germany) and $TiSi_2$ (D_{50}=17.0 μm, purity 99.5%, Beijing Huawei Ruike Chemical Co., Ltd) were used as the experimental materials. To explore the effect of $TiSi_2$ addition on the properties of B_4C composite ceramics, the experimental group, as shown in Table 1, was set up.

The two raw materials were mixed in ethanol with agate balls for 12 h in a plastic bottle, dried at 60 ℃ in a rotating evaporator, and sieved through a 200-mesh sieve. The powder mixtures were poured into a graphite die/punch device (diameter = 50 mm) lined with a 0.3-mm-thick graphite foil. The final composites were produced at a temperature of 2 000 ℃ under a pressure of 30 MPa for 30 min. The heating rate was 10 ℃/min.

Table 1 The experimental setup

Sample number	$TiSi_2$/wt%	Theoretical volume fraction of the product/%	
		SiC	TiB_2
B0	0	0.0	0.0
B5	5	3.1	1.9
B10	10	6.4	3.8
B15	15	9.7	5.8
B20	20	13.1	7.9

Thermal gravimetry (TG) and differential scanning calorimetry (DSC) were used for thermal analyses of the mixed powder to determine whether the reaction occurred. A Vickers indentation test was carried out with a load of 9.8 N and loading time of 15 s on the polished surface. The three-point bending strength was tested on bars of dimensions 3 mm × 4 mm × 36 mm with a span of 30 mm. The fracture toughness was determined according to the single-edge notched beam method using a bar of 3 mm × 5 mm × 25 mm having a 2.5 mm deep and 0.2 mm wide notch. The microstructures and phase components were investigated using scanning electron microscopy (SEM), transmission electron microscopy (TEM), and X-ray diffraction (XRD).

The density of the samples was measured using the Archimedes method. The polished samples were placed in distilled water and boiled for two hours to eliminate pores on the surface of the sample. Then we used a density balance (accuracy 0.000 1 g, Sartorius Mechatronics T&H GmbH) to measure the dry weight $\omega(a)$ and floating weight $\omega(f)$ of the sample, and recorded the water temperature T during the measurement. The sample density was obtained by the following formula:

$$\rho=\frac{\omega(a)\times[\rho(f)-\rho(a)]}{0.999\ 83\times[\omega(a)-\omega(f)]}+\rho(a) \tag{1}$$

In the formula, $\omega(a)$ is the mass of the sample to be tested in air (g); $\omega(f)$ is the mass of the sample to be tested in water (g); $\rho(a)$ is the density of air (g/cm^3); $\rho(f)$ is the density of water(g/cm^3)

3 Results and discussion

3.1 Thermodynamic and kinetic process analyses

According to the literature reports, the possible products were TiSi, Ti_5Si_3[16,17], TiB_2, TiB, TiC, and SiC[18,19] in the B_4C-$TiSi_2$ system, and the possible chemical reactions were suggested by the following equations:

$$B_4C+4TiSi_2+7C\rightarrow 4TiB+8SiC \tag{2}$$

$$B_4C+2TiSi_2+3C\rightarrow 2TiB_2+4SiC \tag{3}$$

$$TiSi_2+C\rightarrow TiSi+SiC \tag{4}$$

$$5TiSi_2+7C\rightarrow Ti_5Si_3+7SiC \tag{5}$$

$$TiSi_2+3C\rightarrow TiC+2SiC \tag{6}$$

The carbon in the reactions is derived from the carbon environment provided by the carbon paper and graphite molds. Because the smaller amount of $TiSi_2$ added in the experiment resulted in a lower carbon content corresponding to the compensation required, no additional carbon was added.

According to the thermodynamics manual, the Gibbs free energies of the reactions were calculated, as shown in Fig.1 (a). All the above reactions are possible, and the most likely reactions are Eq.(2). and Eq.(3).

To confirm the reaction process, DSC and XRD characterizations of the mixed powder corresponding to the sintering temperature were carried out; the results are shown in Fig.1 (b) and (c). There were endothermic peaks near 1 100 and 1 400 ℃, indicating a multi-step reaction. According to the DSC curve, the mixed powder was heated to a temperature at which a reaction may occur, then XRD analyses were performed. At 1 000 ℃, the powder contains $TiSi_2$, B_4C, and slight amounts of TiB_2 and C formed by the reaction. $TiSi_2$ disappears completely at 1 200 ℃. Si formed at 1 100 ℃ and disappeared at 1 300 ℃. A small amount of SiC was formed at 1 300 ℃. After heating at 1 450 ℃, the

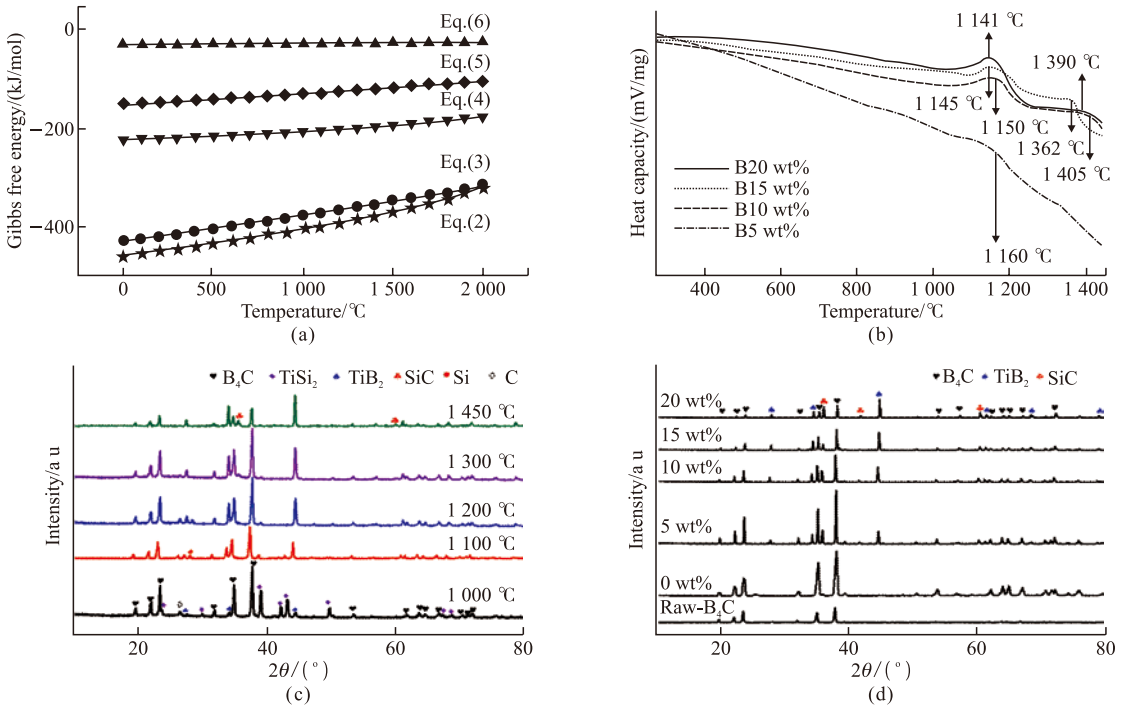

Fig.1 (a) The Gibbs free energy of each formula, (b) DSC curve of mixed powder, (c) XRD pattern of B10 powder at the temperature corresponding to the peak of DSC curve, (d) XRD patterns of the composite materials with different proportions

powder only contains TiB_2, B_4C and SiC. The reaction between Ti and B occurs at 1 000 ℃, while Si and C react at 1 300 ℃. Comparing the two endothermic peaks of the DSC curve, it is suggested that the 1 400 ℃ peak is due to the melting of unreacted Si, which has been reported in the literature[20]. The endothermic peak at 1 150 ℃ may have been caused by the precipitation of Si.

The XRD patterns of the samples are presented in Fig.1(d). B_4C-TiB_2-SiC ceramic composites were successfully synthesized *in situ* by the reactive hot-pressing process. Except for TiB_2 and SiC, no other phases were detected in the XRD patterns shown in Fig.1(d), implying a complete conversion of the raw materials to the product. Thus, we determined that the reaction is Eq.(3). The specific details of this process are discussed in Section 3.4.

3.2 Sintering densification process

Fig.2 shows the relative density, densification curve, and temperature curve of the composite powder with different proportions of $TiSi_2$ during the hot pressing and sintering processes.

When the heating time is 1.5 to 1.7 h, the corresponding temperature is 900-1 000 ℃, and the relative density curves have a stepped drop that indicates the expansion of the composite. According to previous analysis, Ti and B react to form TiB_2. Therefore, it is considered that the expansion is due to the formation of TiB_2, C, and Si. Owing to the varying compositions of the different samples, the expansion temperatures were slightly different. The sintering time was within 2.5 h, when the temperature was below 1 400 ℃, the relative density of the sample increased slowly, and the increased density was less than 1%. The shrinkage below 1 400 ℃ was mainly caused by particle rearrangement or particle slippage. In the temperature range of 1 400-2 000 ℃, the densification rate of all samples increased rapidly, and the more $TiSi_2$ is added to the sample, the greater the slope of the curve.

We speculate that $TiSi_2$ can promote sintering due to these three reasons: 1. Part of the Si reacted with C at 1 300 ℃, and unreacted Si melted during the sintering process, according to the DSC curve. The appearance of the liquid phase and reaction activation accelerated the proton diffusion process and promoted the sintering of B_4C. 2. The consumption of B atoms in B_4C leads to non-stoichiometric B_4C during the reaction, resulting in atomic vacancies and structural defects in the B_4C unit cell. This defect is conducive to the mass transfer process and promotes sintering densification, but it also leads to the growth of B_4C particles. 3. The products SiC generated by the reaction are generally spherical or quasi-spherical, which can promote the rearrangement and flow slip of B_4C particles, thereby reducing the distance between particles and increasing the sintering rate. Within 30 min of the final dwelling, the increase in

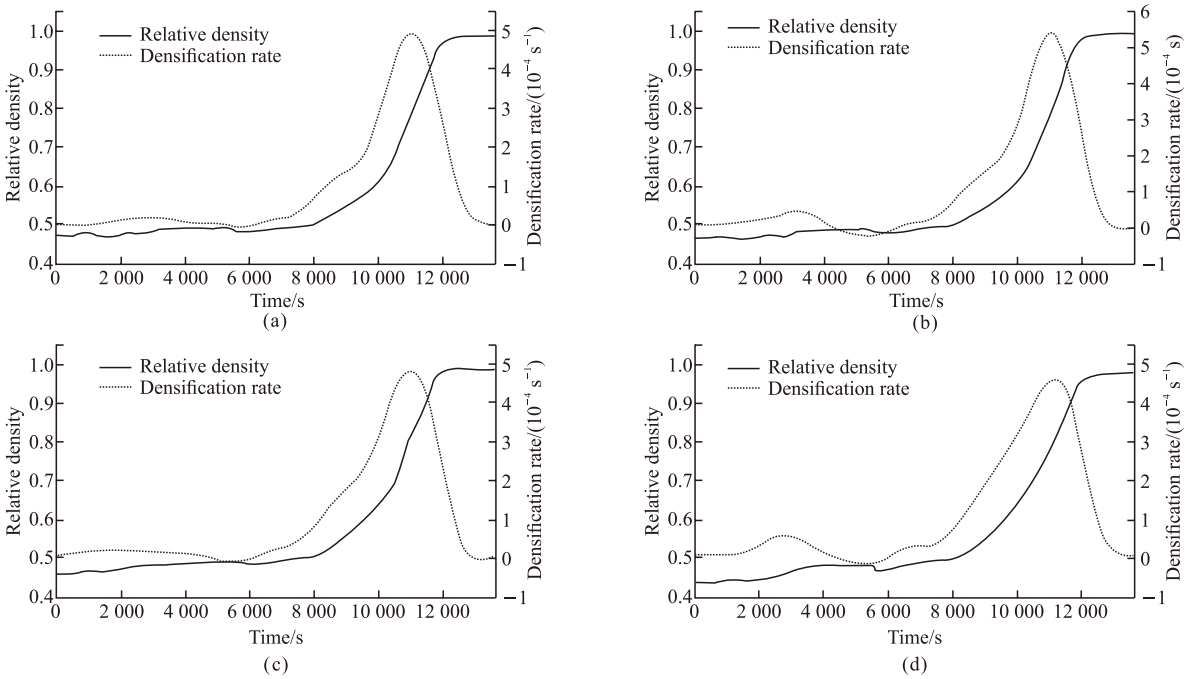

Fig.2 Densification rate of each sample: (a) B5; (b) B10; (c) B15; (d) B20

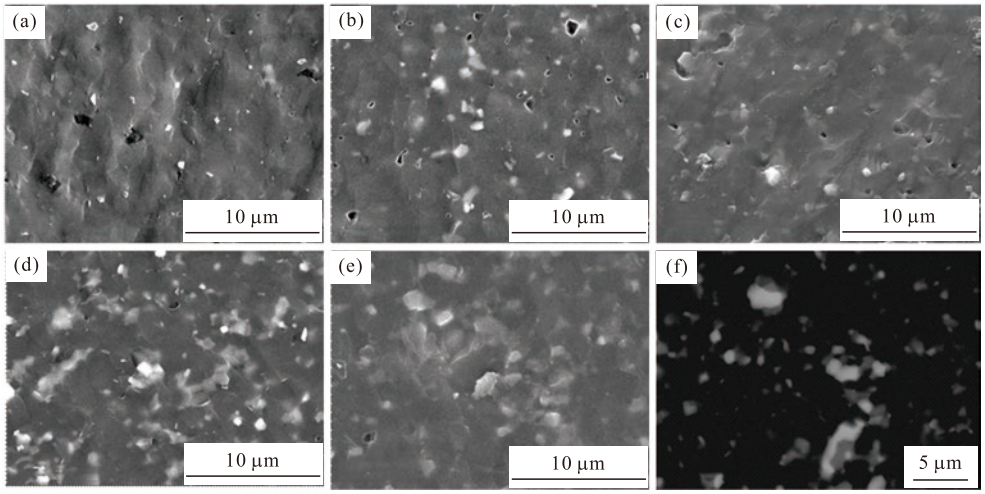

Fig.3 SEM images of sample cross section: (a) B0; (b) B5; (c) B10; (d)B15; (e) B20; (f) BSE image of B10

the relative density decreased again. At the later stage of sintering, densification is mainly achieved through grain boundary diffusion and volume diffusion.

3.3 Microstructure and mechanical properties

Fig.3 shows the microstructures of the composites. According to the SEM images, there were few pores in the B0 section. The pores decrease from (b) to (e) until B20, which does not contain pores. This illustrates that $TiSi_2$ effectively improved the density of the ceramics. A comparison of Fig.3 (b), (c), (d), and (e) shows that when more SiC and TiB_2 were generated, the grains of SiC and TiB_2 increased significantly, and the ceramic section also changed from smooth to rough. This is because the introduction of SiC and TiB_2 changed the fracture mode of the ceramics.

There are three phases in the BSE diagram of B10 (Fig.3 (f)). According to the energy spectrum analysis, the black background is the matrix B_4C, the bright white particles are TiB_2, and the gray particles are SiC. The backscattering pattern shows that a large number of agglomerates of TiB_2 and SiC interspersed with each other are formed in the sample. The average particle size of the added $TiSi_2$ was 17 μm, which had no apparent relationship with the sizes of SiC, TiB_2, and aggregates generated, and the particle sizes of B_4C powder used in different samples were similar (1 μm), indicating that the increase in the generated particle size was

only related to the amount of the added $TiSi_2$.

Fig.4 shows the SEM image of the polished surface of the sample from which the grain size information of the sample can be obtained. The particle sizes of the added SiC and TiB_2 increase with the increase in the $TiSi_2$ content, along with that of the B_4C grains of the sample matrix. The average grain sizes from (a) to (e) were 1.09, 1.23, 1.31, 1.42, and 1.61 μm. The reason is that the reaction between $TiSi_2$ and B_4C increases the sintering activity of the powders, and liquid phase Si is formed during the sintering process, which is beneficial to accelerate the mass transfer process of the powders and leads to the grain growth of B_4C.

The density, hardness, strength, and toughness of the samples are shown in Fig.5. Fig.5 (a) shows that the relative density of all samples is above 98%. Fig.5 (b) shows that the Vickers hardness of the sample is negatively correlated with the $TiSi_2$ content. This is because the hardness of the introduced second phase is lower than that of B_4C. However, the hardness value of the sample does not decrease significantly because the total volume of the generated SiC and TiB_2 content is less than 21%.

The flexural strength of the samples varied with the amount of added $TiSi_2$, as shown in Fig.5 (c). The flexural strength of sample B10 reached its highest value of 807 MPa. As the $TiSi_2$ content increased further, the flexural strength began to decrease. However, when the added amount was 20 wt%, the flexural strength of the sample began to increase again. This is because the flexural strengths of the added SiC and TiB_2 are higher than that of B_4C, increasing the flexural strengths of the three samples B0, B5, and B10, with the generation of SiC and TiB_2 particles.

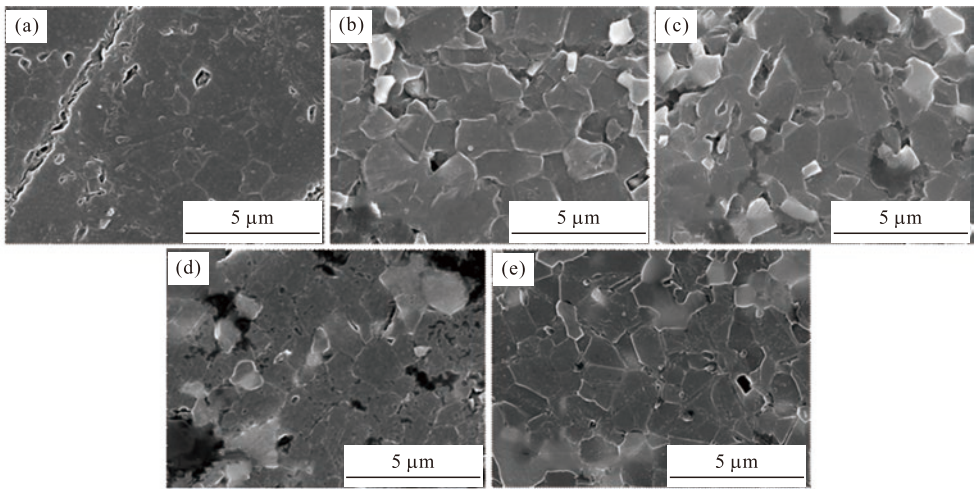

Fig.4 SEM images of etched samples: (a) B0; (b) B5; (c) B10; (d) B15; (d) B20

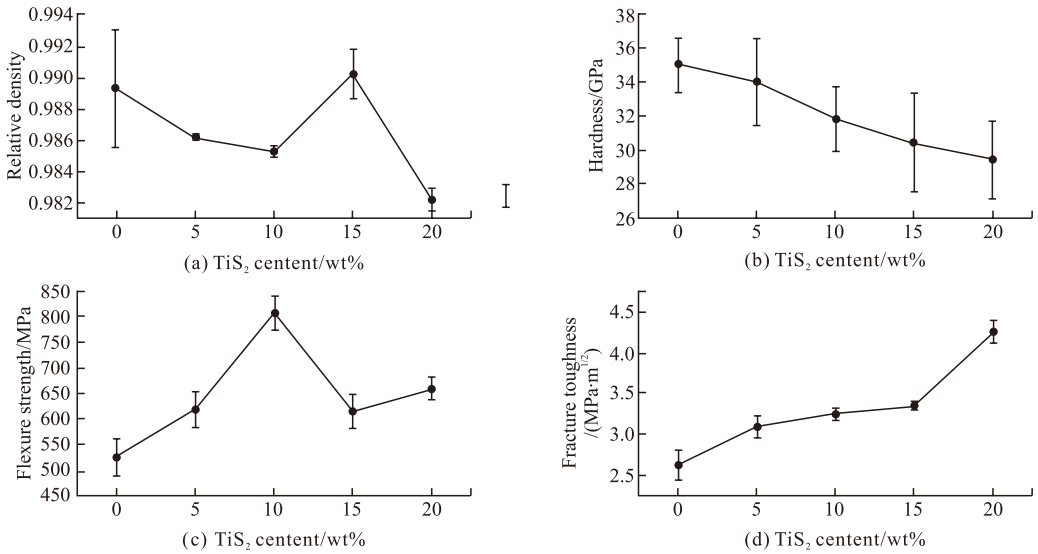

Fig.5 Mechanical properties of the sample: (a) the relative density, (b) the Vickers hardness, (c) the flexural strength, (d) the fracture toughness

However, according to the etching images of the samples in Fig.4, the B_4C grain size increases with the increase in $TiSi_2$ content. An increase in the matrix grain size reduces the flexural strength of the material. The growth of the sample grains from B0 to B10 is small, the increase in the matrix grain size has a negligible effect on the strength, and the introduction of the second phase has a significant impact on the strength of the sample. For sample B15, the B_4C matrix crystal grains grew significantly, resulting in a decrease in strength. The flexural strength of sample B20 increased again because of the higher amounts of SiC and TiB_2, causing the increase in strength to be greater than the decrease in strength caused by the increase in B_4C crystal grains. The final result was that the flexural strength was higher than that of B15 but lower than that of B10. This phenomenon can be explained based on the competition between the two mechanisms of the growth of the ceramic matrix B_4C grains, leading to a decrease in the overall strength and an increase in the added SiC and TiB_2, leading to an increase in the overall strength.

Fig.5 (d) shows that the fracture toughness of pure B_4C ceramics is the lowest (2.8 MPa•$m^{1/2}$). For sample B20, the value is 4.2 MPa•$m^{1/2}$, corresponding to the maximum.

The fracture mode when the crack penetrates the composite material is shown in the Fig.6. It can be seen that transgranular fracture occurs when the crack passes through SiC-B_4C, and intergranular fracture occurs when through B_4C-TiB_2 and SiC-TiB_2. Good interface compatibility and similar coefficients of thermal expansion between SiC (4.7×10^{-6} K) and B_4C (4.5×10^{-6} K) in the sample lead to transgranular fracture when the crack passes through[21]. Because the fracture toughness of SiC is higher than that of B_4C, more energy will be consumed when the crack penetrates, which can be understood as improving the plastic deformation ability of the matrix material. An intergranular fracture occurs when the crack passes through TiB_2-B_4C and TiB_2-SiC, which is attributed to the mismatch between the thermal expansion coefficients of TiB_2 and the other two phases. This fracture mode of B_4C-TiB_2 and SiC-TiB_2 leads to toughening by extending the crack propagation path and consuming crack propagation energy[22,23]. Because the agglomerate structure of the interspersed small particles of SiC and TiB_2 can guide the crack to exhibit larger deflection, significantly improving the mechanical properties of the composite material.

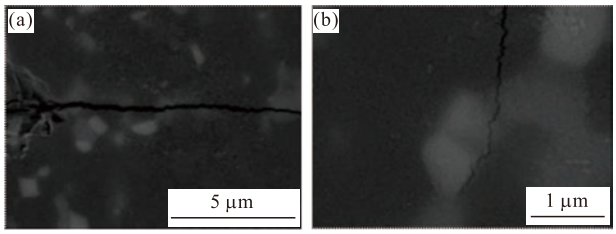

Fig.6 Different fracture modes when cracks pass through composite materials: (a)B_4C-SiC; (b) B_4C- TiB_2, SiC-TiB_2

3.4 Microscopic reaction process

To understand the TiB_2-SiC agglomerate structure, focused ion beam(FIB) was used to cut it, and TEM and EDS surface scans were performed. The results are shown in Fig.7 TEM results showed that the TiB_2-SiC agglomerate was formed by interspersing several SiC and TiB_2 crystal grains. The electron diffraction pattern

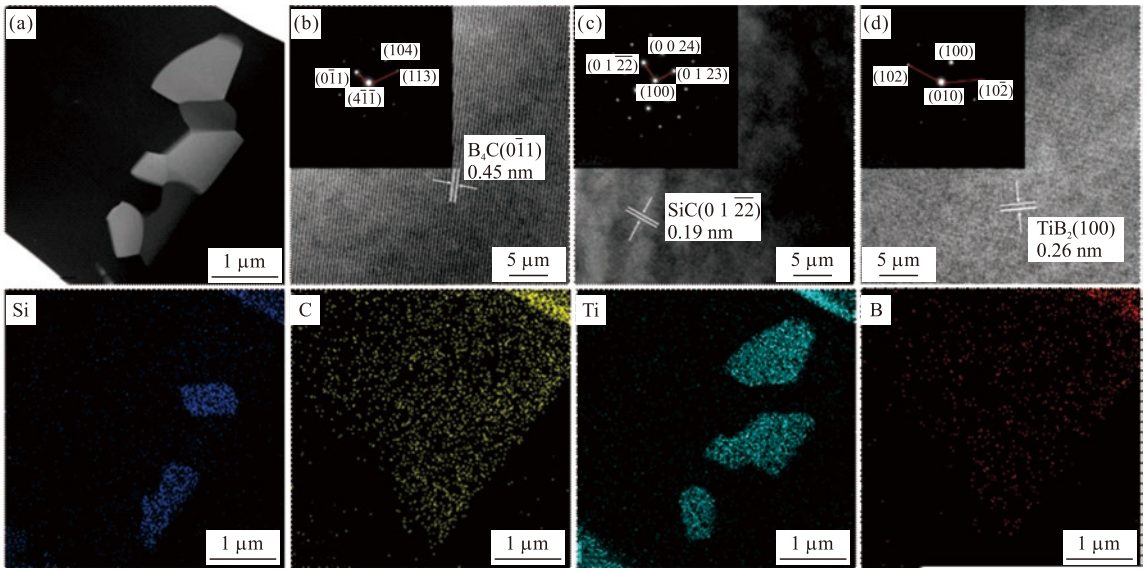

Fig.7 TEM image and EDS scan of TiB_2-SiC agglomeration structure: (a) FIB image of cutting; (b) B_4C; (c) SiC; (d) TiB_2

in Fig.7 (c) shows that the generated SiC has a hexagonal crystal structure.

A diffusion couple experiment of $TiSi_2$ and B_4C compact blocks at 1 300 ℃ was performed to observe the diffusion of atoms at the reaction temperature. The elemental analysis of the diffusion couple interface shows that there is atomic migration, as shown in Fig.8. The delamination of Si and Ti element can be clearly observed in this image. Energy dispersive spectroscopy (EDS) line scan was performed on the reaction interface of $TiSi_2$ and B_4C to analyze the diffusion of elements, and the results are shown in Fig.9.

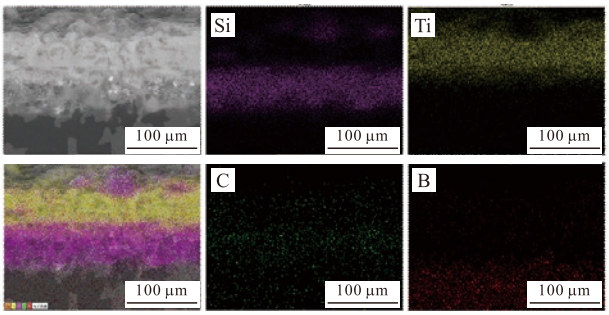

Fig 8 Mapping of $TiSi_2$ and B_4C reaction interface

The diffusion curve can be divided into three sections: 1. There are only three elements, B, C, and Ti, in the 0-2 μm region. Only Ti was detected at the $TiSi_2$ interface. B atoms diffuse into $TiSi_2$ and react with Ti to form TiB_2. Due to the atomic concentration, a small amount of C atoms also diffused into this area, but no reaction occurred. 2. There are four elements, Ti, B, C, and Si, in the 1.5-3.5 μm region. Combining the atomic ratio of the energy spectrum, the reaction temperature of each element, and the XRD phase analysis of the mixed powder at the corresponding temperature, it is detected the products contained in this region are TiB_2, Si, C, and B_4C. 3. There are three elements, B, C, and Si, in the 3.5-6.5 μm region, and Ti atoms did not diffuse into B_4C. According to the XRD and EDS line scan results, this area contains B_4C, Si, and C. Therefore, at 1 300 ℃, from $TiSi_2$ to the B_4C side, the intermediate diffusion layers are in the order TiB_2, C/TiB_2, Si, C/B_4C, C, and Si.

Owing to the varying atomic concentrations, B and C atoms in B_4C and Ti and Si atoms in $TiSi_2$ diffuse toward each other. Lighter atoms have faster diffusion rates, therefore, the diffusion rate of B atoms is greater than that of C atoms and the diffusion rate of Si was greater than that of Ti atoms. B atoms diffuse to the TiB_2 vicinity of Ti atoms and initiate the reaction, forming a product layer. Si and C do not react at 1 300 ℃ under normal pressure.

Based on the above experimental results, we describe the entire reaction process under atmospheric pressure, and the schematic diagram is shown in Fig.10.

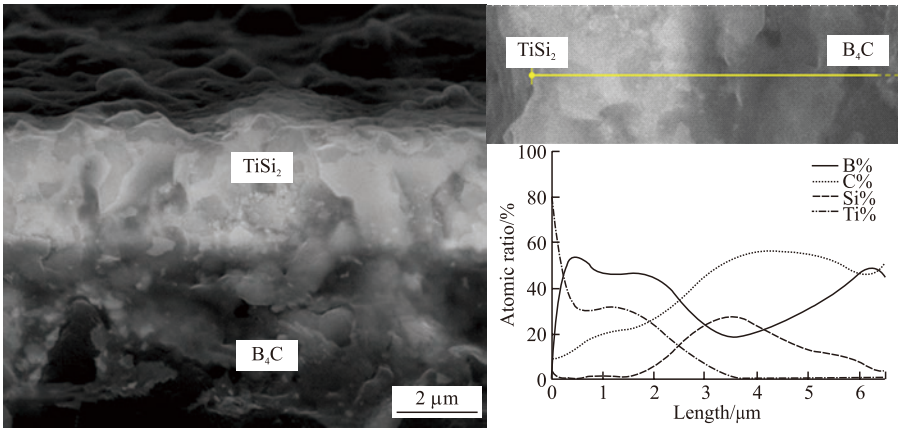

Fig.9 EDS line scan at the reaction interface of $TiSi_2$ and B_4C

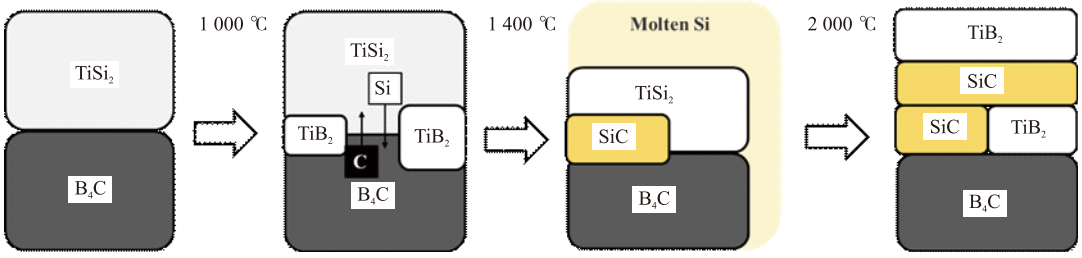

Fig.10 Reaction process diagram of B_4C and $TiSi_2$

The Ti atoms in $TiSi_2$ and B atoms in B_4C react to form TiB_2, leaving C at 1 000 ℃. $TiSi_2$ is completely disappeared at 1 200 ℃. Then as the temperature increases, the diffusion rate of atoms is accelerated, more TiB_2 is generated, and Si and C contents also increase. At 1 300 ℃, a small amount of Si in the powder mixture begin to react with C to form SiC. At 1 400 ℃, melting of Si was initiated. The liquid-phase Si fills the gap between the B_4C and TiB_2 particles and provides a new channel for atomic diffusion, then reacts completely to form SiC. Finally it leads to the formation of a large number of SiC and TiB_2 phase aggregates.

4 Conclusions

In this study, an *in situ* reaction hot-pressing sintering process was employed, and $TiSi_2$ was used as an additive to prepare high-hardness and high-strength B_4C-SiC-TiB_2 composite ceramics at 2 000 ℃.

During the sintering process, the reaction between $TiSi_2$ and B_4C was controlled by the diffusion rate of the atoms. The reaction starteds at 1 000 ℃ to produce TiB_2, free Si, and C; part of the Si reacteds with C to form SiC at the temperature of 1 300 ℃, and unreacted Si began to melt at approximately 1 400 ℃. The melted Si surrounded TiB_2, B_4C, and other products and filled the gaps between the particles, forming a large amount of the second phase structure of SiC-TiB_2 agglomerates. This type of SiC-TiB_2 interspersed agglomerate structure can significantly enhance the mechanical properties of B_4C. By adding different mass fractions of $TiSi_2$, B_4C-SiC-TiB_2 composite ceramic with high strength of 806 MPa and modest fracture toughness of 3.2 $MPa{\cdot}m^{1/2}$ could be achieved.

References

[1] Thévenot F. Boron Carbide-a Comprehensive Review[J]. *J. Eur. Ceram. Soc.*, 1990, 6(4): 205-225

[2] Suri AK, Subramanian C, Snober JK, *et al*. Synthesis and Consolidation of Boron Carbide: A Review[J]. *Int. Mater. Rev.*, 2010, 55(1): b4-40

[3] Wang S, Xing P, Gao S, *et al*. Effect of *in-situ* Formed CrB_2 on Pressureless Sintering of B_4C[J]. *Ceram. Int.*, 2018, 44(16): 20 367-20 374

[4] Rehman SS, Wei J, Fu Z, *et al*. *In situ* Synthesis and Sintering of B_4C/ZrB_2 Composites from B_4C and ZrH_2 Mixtures by Spark Plasma Sintering[J]. *J. Eur. Ceram. Soc.*, 2015, 35(4): 1 139-1 145

[5] Xiong Y, Du X, Xiang M, *et al*. Densification Mechanism during Reactive Hot Pressing of B_4C-ZrO_2 Mixtures[J]. *J. Eur. Ceram. Soc.*, 2018, 38(12): 4 167-4 172

[6] Tang J, Ji W, Xie J, *et al*. Fine and High-performance $B_{6.5}C$-TiB_2-SiC-BN Composite Fabricated by Reactive Hot Pressing Via TiCN-B-Si Mixture[J]. *Ceram. Int.*, 2020, 46(8): 11 013-11 020

[7] Deng JX, Sun JLX. Microstructure and Mechanical Properties of Hot-pressed B_4C/TiC/Mo Ceramic Composites[J]. *Ceram. Int.*, 2009, 35(2): 771-778

[8] Wang S, Gao S, Xing P, *et al*. Pressureless Liquid-phase Sintering of B_4C with $MoSi_2$ as a Sintering Aid[J]. *Ceram. Int.*, 2019, 45(10): 13 502-13 508

[9] Zhang ZX, Xu CJ, Du XW, *et al*. Synthesis Mechanism and Mechanical Properties of TiB_2-SiC Composites Fabricated with the B_4C-TiC-Si System by Reactive Hot Pressing[J]. *J. Alloys Compd.*, 2015, 619: 26-30

[10] Cao YQ, He QL, Wang WM, *et al*. Microstructure, Mechanical, and Thermal Properties of B_4C-TiB_2-SiC Composites Prepared by Reactive Hot-pressing[J]. *J. Wuhan Univ. Technol.*, 2020, 35: 1 031-1 037

[11] Moshtaghioun BM, Ortiz AL, Gómez-Garcja D, *et al*. Toughening of Super-hard Ultra-fine Grained B_4C Densified by Spark-plasma Sintering Via SiC Addition[J]. *J. Eur. Ceram. Soc.*, 2013, 33(8): 1 395-1 401

[12] Zorzi JE, Perottoni CA, da Jornada JAH. Hardness and Wear Resistance of B_4C Ceramics Prepared with Several Additives[J]. *Mater. Lett.*, 2005, 59(23): 2 932-2 935

[13] Yamada S, Hirao K, Yamauchi Y, *et al*. High Strength B_4C-TiB_2 Composites Fabricated by Reaction Hot-pressing[J]. *J. Eur. Ceram. Soc.*, 2003, 23(7): 1 123-1 130

[14] Zhang XH, Li WJ, Hong CQ, *et al*. Microstructure and Mechanical Properties of ZrB_2-based Composites Reinforced and Toughened by Zirconia[J]. *Int. J. Appl. Ceram. Technol.*, 2008, 5(5): 499-504

[15] Gutmanas EY, Gotman I. Reactive Synthesis of Ceramic Matrix Composites under Pressure[J]. *Ceram. Int.*, 2000, 26(7): 699-707

[16] Hoke DA, Kim DK, Lasalvia JC, *et al*. Combustion Synthesis/Dynamic Densification of TiB_2-SiC Composite[J]. *J. Am. Ceram. Soc.*, 1996, 79(1): 177-182

[17] Raju GB, Basu B. Densification, Sintering Reactions, and Properties of Titanium Diboride with Titanium Disilicide as a Sintering Aid[J]. *J. Am. Ceram. Soc.*, 2007, 90(11): 3 415-3 423

[18] Liu GQ, Chen SX, Zhao YW, *et al*. Effect of Ti and Its Compounds on the Mechanical Properties and Microstructure of B_4C Ceramics Fabricated Via Pressureless Sintering[J]. *Ceram. Int.*, 2021, 47(10): 13 756-13 761

[19] Xu CM, Hong Z, Zhang GJ. Pressureless Sintering of Boron Carbide Ceramics with Al-Si Additives[J]. *Int. J. Refract. Met. H*, 2013, 41: 2-6

[20] Du XW, Wang Y, Zhang ZX, *et al*. Effects of Silicon Addition on the Microstructure and Properties of B_4C-SiC Composite Prepared with Polycarbosilane-coated B_4C Powder[J]. *Mater. Sci. Eng. A*, 2015, 636: 133-137

[21] King DS, Fahrenholtz WG, Hilmas GE. Silicon Carbide-titanium Diboride Ceramic Composites[J]. *J. Eur. Ceram. Soc.*, 2013, 33(15-16): 2 943-2 951

[22] Zhang XR, Zhang ZX, Wang WM, *et al*. Microstructure and Mechanical Properties of B_4C-TiB_2-SiC Composites Toughened by Composite Structural Toughening Phases[J]. *J. Am. Ceram. Soc.*, 2017, 100(7): 3 099-3 107

[23] Zhang XR, Zhang ZX, Liu YM, *et al*. High-performance B_4C-TiB_2-SiC Composites with Tuneable Properties Fabricated by Reactive Hot Pressing[J]. *J. Eur. Ceram. Soc.*, 2019, 39(10): 2 995-3 002